# Chapter 5
# Observation Weighting Using Signal Quality Measures

In addition to pseudo-range and carrier-phase measurements, a modern geodetic-type GPS receiver also records signal-to-noise ratio (SNR) data. Relying upon signal quality measures, the heteroscedasticity (i.e., inhomogeneity of variances) of GPS phase observations can be more realistically described than using the satellite elevation angle. Section 5.1 gives a brief introduction to SNR and numerical examples of how various factors affect its characterisation. Next, in Sect. 5.2, different SNR-based weighting schemes are reviewed, with a particular focus on their strengths and weaknesses. Section 5.3 presents an empirical SNR-based weighting model and its implementation in the Bernese GPS Software 5.0. The proposed approach is compared with the commonly applied elevation-dependent weighting scheme and two other SNR-based alternatives. Finally, in Sect. 5.4, the main properties of the novel SNR-based weighting model are summarised from both theoretical and practical points of view.

## 5.1 Signal-to-Noise Ratio

The notation SNR represents a generic term for signal quality and is defined as the ratio of signal power $S$ in watts (W) to noise power $N$ in W, measured at the same time and place in a circuit. The signal and noise power can be estimated during the synchronisation (or correlation) between the received and replica signals (Butsch and Kipka 2004). The main part of noise originates from the receiver electronics (e.g., thermal noise created by the inevitable motion of electrons within any conductor or semiconductor) and the electromagnetic radiation from the sky, ground and objects in the antenna's vicinity. Thermal noise is generally assumed to be uncorrelated (white) noise with a Gaussian distribution (Langley 1997). Intuitively, the larger the $SNR = S/N$ value, the better the signal quality.

Normally, SNR measurements are obtained using the signal power $S_{corr}$ and noise power $N_{corr}$ of the modulated signal at the correlator output, indicating that

X. Luo, *GPS Stochastic Modelling*, Springer Theses,
DOI: 10.1007/978-3-642-34836-5_5, © Springer-Verlag Berlin Heidelberg 2013

$SNR = S/N = S_{corr}/N_{corr}$. However, to assess the quality of a received GPS signal, the so-called carrier-to-noise ratio ($CNR = C/N$) is preferred, which makes use of the signal power $C_{ant}$ and noise power $N_{ant}$ of the unmodulated carrier at the receiving antenna (i.e., $CNR = C/N = C_{ant}/N_{ant}$; Ward et al. 2006, p. 185). From the receiver antenna to correlator output, GPS signals may be amplified by a factor of about $10^{10}$, so that $S_{corr}$ is significantly larger than $C_{ant}$ (Butsch and Kipka 2004). Nevertheless, according to the fact that the signal and noise powers are amplified by approximately the same factor, $S_{corr}/N_{corr}$ and $C_{ant}/N_{ant}$ are almost identical, i.e.,

$$CNR := \frac{C}{N} = \frac{C_{ant}}{N_{ant}} \approx \frac{S_{corr}}{N_{corr}} = \frac{S}{N} =: SNR. \tag{5.1}$$

For GPS signals, $S$ is several magnitudes lager than $N$. Therefore, SNR values are usually expressed in terms of the logarithmic decibel (dB) scale by

$$SNR\,[\mathrm{dB}] = 10 \cdot \log_{10}(SNR). \tag{5.2}$$

In addition, noise power $N$ can be written as the product of noise power density $N_0$ and loop bandwidth $B_L$ (Misra and Enge 2006, p. 403):

$$N\,[\mathrm{W}] = N_0\,[\mathrm{W/Hz}] \cdot B_L\,[\mathrm{Hz}]\,, \tag{5.3}$$

where $B_L$ is commonly the same on L1 and L2 for GPS receivers (Lau and Mok 1999). Substituting Eq. (5.3) into (5.1), $SNR$ is normalised to a specific bandwidth of 1 Hz, and Eq. (5.2) becomes

$$\begin{aligned} SNR\,[\mathrm{dB}] &= 10 \cdot \log_{10} \frac{S}{N_0 \cdot B_L} = 10 \cdot \log_{10} \left( \frac{S}{N_0} \right) - 10 \cdot \log_{10}(B_L) \\ &= SNR0\,[\mathrm{dBHz}] - B_L\,[\mathrm{dBHz}]\,, \end{aligned} \tag{5.4}$$

where $SNR0$ (or $S/N_0$) is called signal-to-noise power density ratio. It plays a key role in analysing GPS receiver performance and is directly related to the precision of pseudo-range and carrier-phase observations (Langley 1997). For moderate to strong signals, the corresponding $SNR0$ should be larger than 35 dBHz (Hofmann-Wellenhof et al. 2008, p. 86). Most high-end GPS receivers deliver $SNR0$ of up to 50 dBHz. Using the minimum received signal strength of $S = -160$ dBW and a typical value for noise power density of $N_0 = -204$ dBW/Hz (IS-GPS-200E 2010, p. 15), a nominal $SNR0$ of 44 dBHz is obtained.

In fact, $SNR0$ measurements are affected by various factors, for example, (1) the antenna gain of the transmitting satellite and thus by the satellite type, (2) polarisation errors, (3) the size of solar panels and batteries, (4) changes in path (spreading) loss due to the varying satellite-receiver distance, (5) variations in atmospheric attenuation and receiver antenna gain patterns, depending on the elevation angle and azimuth of the arriving signal, and (6) signal power losses in preamplifier, antenna cable

and receiver subsystems. Furthermore, the noise level may be slightly increased by the signals from other simultaneously observed satellites (Langley 1997). Table 5.1 provides numerical examples of signal power losses, transmitter and receiver antenna gains, as well as the typical noise characterisation of a GPS receiver (Misra and Enge 2006, Chap. 10).

Taking the C/A-code on L1 as an example, a GPS satellite transmits a signal power of about 27 W, corresponding to $P_S = 10 \cdot \log_{10}(27) = 14.3$ dBW. This power level is derived from GPS specifications, and typical GPS satellites broadcast 2–4 dB more power (3 dB: twice as powerful; Misra and Enge 2006, p. 395). Assuming that the GPS signals were transmitted in all directions, path loss describes the spreading of the total signal energy over the entire surface area of the sphere, which is centred on the satellite. The path loss can be expressed by $L_P = 4\pi R^2$, where $R$ is the satellite-receiver distance, computed based on the satellite elevation angle $e$ and approximate values of the Earth's and orbital radii, $R_E = 6{,}371$ km and $R_S = 26{,}560$ km, respectively. For a satellite in the zenith direction, i.e., $e = 90°$ and $R = R_S - R_E = 20{,}189$ km, the resulting $L_P$ is 157.1 dBm$^2$, corresponding to a power attenuation of about $2.0 \times 10^{-16}$/m$^2$. Since a GPS satellite focuses its signal energy towards the Earth, satellite antenna gain (or concentration factor) char-

**Table 5.1** Typical values for signal power losses, transmitter and receiver antenna gains and noise characterisation of a GPS receiver (Misra and Enge 2006, Tables 10.1–10.4)

| **Signal characterisation** | **Notation** | **Unit** | $e = 5°$ | $e = 40°$ | $e = 90°$ |
|---|---|---|---|---|---|
| Power (satellite antenna input) | $P_S$ | dBW | 14.3 | 14.3 | 14.3 |
| Satellite-antenna distance | $R$ | km | 25,235 | 22,013 | 20,189 |
| Path (spreading) loss | $L_P$ | dBm$^2$ | 159.0 | 157.8 | 157.1 |
| Satellite nadir angle | $\alpha$ | degree | ±13.8 | ±10.6 | ±0 |
| Satellite antenna gain | $G_S$ | dB | 12.1 | 12.9 | 10.2 |
| Atmospheric loss | $L_A$ | dB | 2.0 | 0.5 | 0.5 |
| Received power density | $PD_R$ | dBW/m$^2$ | −134.6 | −131.1 | −133.1 |
| Effective area of an IRA[a] | $A_R(IRA)$ | dBm$^2$ | −25.4 | −25.4 | −25.4 |
| Received power for an IRA | $P_R(IRA)$ | dBW | −160.0 | −156.5 | −158.5 |
| Receiver antenna gain | $G_R(IRA)$ | dB | −4 | 2 | 4 |
| **Noise characterisation** | **Notation** | **Unit** | **Bef. LNA**[b] | **LNA** | **Aft. LNA** |
| Power gain | $G_i$ | dB | −1 | 20 | −10 |
| Power loss (1/gain) | $L_i$ | dB | 1 | −20 | 10 |
| Noise figure | $F_i$ | dB | 1 | 3 | 10 |
| **Power (C/A-code signal)** | **Notation** | **Unit** | $e = 5°$ | $e = 40°$ | $e = 90°$ |
| Received signal power | $S$ | dBW | −164.0 | −154.5 | −154.5 |
| Noise power density | $N_0$ | dBW/Hz | −201 | −201 | −201 |
| Power density ratio | $SNR0$ | dBHz | 37.0 | 46.5 | 46.5 |
| Signal-to-noise (power) ratio | $SNR$ | dB | −36.0 | $B_L = 20$ MHz | −26.5 |
| | | | 4.0 | 2 KHz | 13.5 |
| | | | 34.0 | 2 Hz | 43.5 |

[a] IRA: isotropic receiver antenna
[b] LNA: low noise amplifier

acterises the amplification of the signal power in a certain direction with respect to an isotropic antenna. Assuming that the satellite is capable of concentrating its radiated power within the beam angle completely, the satellite antenna gain $G_S$ can be determined as the ratio of the area of the whole sphere to the area of a spherical cap:

$$G_S(\alpha) = \frac{4\pi R^2}{\pi(R\sqrt{2-2\cos\alpha})^2} = \frac{2}{1-\cos\alpha}, \tag{5.5}$$

where $\alpha$ is the satellite nadir angle and can be calculated using $e$, $R_E$ and $R_S$. For $e = 0°$, $\alpha$ reaches a maximum of about 13.9°. In effect, the GPS signal beam has a wider spread of $\alpha = \pm 21.3°$. As a consequence, the maximum satellite antenna gain may be more realistically approximated by $G_S(21.3°) = 14.7$ dB [see Eq. (5.5)]. Moreover, due to the additional power loss in the satellite antenna and the compensation for the larger distance to those areas at the edge of the Earth, the actual satellite antenna gain is less than 14.7 dB and is about 2 dB higher for $\alpha = \pm 13.9°(e = 0°)$ than along the so-called bore sight with $\alpha = \pm 0°(e = 90°)$ (Misra and Enge 2006, p. 397). As an example, for a satellite at zenith with $\alpha = \pm 0°$, the effective radiated power is equal to $P_S + G_S = 14.3$ dBW + 10.2 dB = 24.5 dBW = 282 W.

Within the context of atmospheric loss, $L_A$, oxygen is the dominant source of signal power attenuation at L-band. However, for elevation angles exceeding 40°, the atmospheric loss approaches 0.035 dB and thus can be safely neglected. Other phenomena, such as atmospheric turbulence and water vapour, may sometimes cause additional losses (Betz 2010). Considering the worst-case scenario, $L_A$ is specified to 2 dB for $e = 5°$ (Mehaffey 2011). For a moderate elevation angle and near zenith at which higher received signal power is expected, a representative value of $L_A = 0.5$ dB is used (GPS-SPS-SS 1995, p. 18). Combining the above-introduced factors that impact upon the transmitted signal power, the received power density $PD_R$ is given by

$$PD_R[\mathrm{dBW/m^2}] = P_S\,[\mathrm{dBW}] + G_S\,[\mathrm{dB}] - L_P[\mathrm{dBm^2}] - L_A\,[\mathrm{dB}]\,. \tag{5.6}$$

The received signal power is the product of the received power density in the incident signal field $PD_R$ and the receiver antenna effective area denoted as $A_R$. This term measures the antenna's ability to capture the power in a field incident to a certain direction. It can be calculated based on the receiver antenna gain, $G_R$, which characterises the antenna's ability to focus transmitted power in a certain direction:

$$A_R = \frac{\lambda^2}{4\pi} G_R, \quad \lambda = \frac{c}{f}, \tag{5.7}$$

where $\lambda$ is the wavelength of the signal, $c$ is the speed of light in a vacuum, and $f$ is the frequency of the signal (Jordan and Balmain 1968, p. 377). An isotropic receiver antenna (IRA) is equally sensitive to signals from any direction and has unit gain, indicating $G_R(IRA) = 1$ and $A_R(IRA) = \lambda^2/(4\pi)$. Taking the L1 carrier with a wavelength of about 19 cm as an example, the corresponding $A_R(IRA)$ is equal to

$2.87 \times 10^{-3}\text{m}^2 = -25.4\ \text{dBm}^2$. Assuming that the receiver antenna gain $G_R(IRA)$ is given relative to an isotropic antenna, the received signal power is

$$S\,[\text{dBW}] = \underbrace{PD_R[\text{dBW/m}^2] + A_R(IRA)[\text{dBm}^2]}_{P_R(IRA)[\text{dBW}]} + G_R(IRA)\,[\text{dB}]\,. \tag{5.8}$$

As shown by Misra and Enge (2006, p. 400) and IS-GPS-200E (2010, p. 45), the received C/A-code signal level depends on the satellite elevation angle $e$. As $e$ varies from 5 to 90° (zenith), $P_R(IRA)$ first increases to its maximum of −156.3 dBW at an elevation angle of about 45° and then decreases. Such a variation pattern can also be expected in the received signal power $S$, since for most civilian GPS receiver antennas, $G_R(IRA)$ decreases slowly from about 4 dB at $e = 90°$ to −4 dB at $e = 5°$ (Misra and Enge 2006, p. 401).

The factors that influence the noise power level include the thermal noise generated in the receiver, natural noise from sources outside the receiver, reflected signals (e.g., multipath), signals from other simultaneously observed GPS satellites and the interfering signals from systems other than GPS. Within the context of noise analysis, it is convenient to treat a GPS receiver as a cascade of components (or subsystems), each of which can be characterised by its power gain $G_i$ and noise figure $F_i$. While some components, for example, low noise amplifier (LNA), amplify the signal power, some subsystems, such as cables and connectors before and after the LNA, attenuate signals and have gain values of less than one (i.e., $G_i < 1$). These components with negative $G_i$ values in dB are termed passive. The resulting power loss converts into heat and introduces thermal noise. Noise figure $F_i$ describes the degradation of $SNR0$ as the signal passes through each receiver component. If there is no internal noise, i.e., $F_i = 1$, then the $SNR0$ at the output of the subsystem $i$ is identical with that at the input. For a passive component, $F_i$ is equal to the power loss $L_i$, which represents the inverse of $G_i$. The component before the LNA consists of a low-loss filter that removes signals outside the GPS band, and a short (low-loss) cable that connects the antenna to the LNA (Hofmann-Wellenhof et al. 2008, p. 88). For this part, a low power loss of 1 dB is specified in Table 5.1. The LNA is also designed for high gain and low noise, having a typical gain (noise figure) of 20 dB (3 dB). Due to the following more complex filtering and converting steps, the part after the LNA has a significantly higher power loss of 10 dB. Using these noise characteristics, the noise power density $N_0$ can be determined (Misra and Enge 2006, p. 409). For a typical GPS receiver, $N_0$ is of the order of −201 to −204 dBW/Hz (Hofmann-Wellenhof et al. 2008, p. 86). On the basis of $S$ and $N_0$, the resulting $SNR0$ values vary from 37.0 to 46.5 dBHz for satellites at low and high elevation angles, respectively.

The bandwidth $B_L$ of a GPS receiver is wider for the components near the antenna and becomes narrower as the signal processing proceeds. For instance, the earliest filters in the receiver front end have bandwidths of tens of megahertz. If $B_L = 20\ \text{MHz} = 73\ \text{dBHz}$, the signal power is 26.5 to 36 dB weaker than the noise power, indicating that the GPS signal is below the noise floor. As the processing develops, however, the bandwidth decreases. For a bandwidth of 2 Hz (Langley

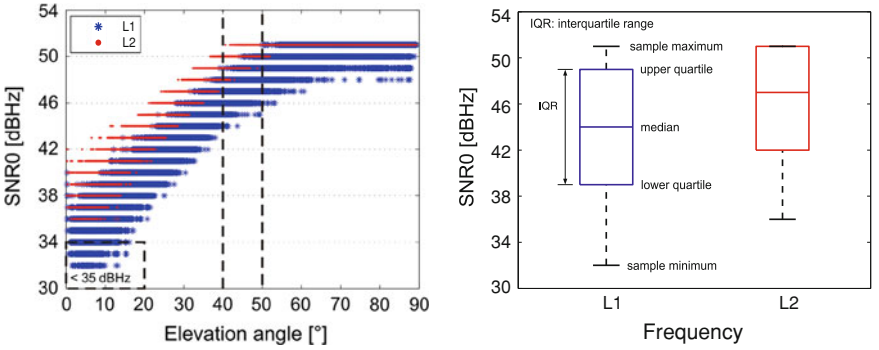


**(a)** *SNR*0 values on L1 and L2 **(b)** Box plots of the *SNR*0 values

**Fig. 5.1** Example of *SNR*0 values in dBHz (SA*POS*®site: RAVE, weak multipath, receiver: Leica SR520, antenna: LEIAT503, DOY2004:186; see Table 4.1)

1997), the GPS signal is about 34.0 to 43.5 dB above the noise floor (see Table 5.1). The technique of increasing signal power by decreasing bandwidth is known as despreading, which is performed by correlators contained in the delay lock loops (Misra and Enge 2006, Sect. 10.5).

Depending on the satellite elevation angle, Fig. 5.1 shows examples of daily *SNR*0 measurements and the associated box plots for a Leica antenna-receiver combination. In Fig. 5.1a, the *SNR*0 values illustrate a strong elevation dependence, with low-quality (i.e., *SNR*0 $< 35$ dBHz; see Fig. 5.6) observations concentrating within the range of $e < 20°$. The staircase-shaped structure of the *SNR*0 values arises from both the resolution of signal quality registration and the derivation of *SNR*0 from the raw observation data (Mayer 2006, p. 63). In comparison to L1, the *SNR*0 values on L2 exhibit a larger minimum (L1: 32 dBHz, L2: 36 dBHz) and a narrower variation range (L1: 19 dBHz, L2: 15 dBHz). These can be easily observed by comparing the sample minima and interquartile ranges (IQR) of the box plots (see Fig. 5.1b). Moreover, the L2 *SNR*0 achieves a maximum of 51 dBHz at an elevation angle of about 40° and maintains it for $e > 50°$, while the L1 *SNR*0 approaches its maximum at about $e = 50°$ and varies within 6 dBHz for higher elevation angles. Applying elevation-dependent observation weighting models (e.g., $\sin^2(e)$), these frequency-related characteristics of signal quality are simply ignored. However, they can be considered by incorporating frequency-dependent signal quality measures into the observation weighting procedure.

Geodetic-type GPS receivers usually provide *SNR* in dB or *SNR*0 in dBHz. However, sometimes the so-called arbitrary manufacturer (mystery) units (AMU), also known as signal-to-noise counts (SNC), are used to assess the quality of GPS signals (e.g., Trimble 4000SSI receivers). These values are obtained by integrating the output of a signal correlator and can vary from receiver to receiver due to the differences in receiver bandwidth and in integration time. To keep the consistency across a product line, *AMU* values are scaled to match a measurement over a bandwidth of

1 kHz. This particular bandwidth is chosen due to the fact that the integration time of a majority of early receivers is 1 ms, corresponding to an effective bandwidth of 1 kHz (Trimble 1999). Applying the manufacturer-specific formula

$$SNR0\,[\text{dBHz}] = 27 + 20 \cdot \log_{10}(AMU), \tag{5.9}$$

*AMU* values, for example, from a Trimble 4000SSI receiver, can be converted into *SNR*0. Note that the converted *SNR*0 only represents an approximation, and biases of up to 3 dBHz are possible, particularly for small *AMU* values at low elevation angles, where the conversion tends to be considerably non-linear (Butsch and Kipka 2004). Figure 5.2 depicts the conversion function Eq. (5.9), along with some satellite- and site-related results for an antenna-receiver combination from the Trimble 4000 series products. Apart from the conversion formula itself, Fig. 5.2a also illustrates the variation in *SNR*0 due to an error of 1 *AMU*, derived by applying the error propagation law to Eq. (5.9). For $AMU < 10$, the conversion exhibits a significantly non-linear behaviour, leading to errors that are considerably larger than 1 dBHz. In Fig. 5.2b, the *AMU* and the converted *SNR*0 values are displayed for a specific satellite, where the elevation angles are obtained from the GPS navigation message

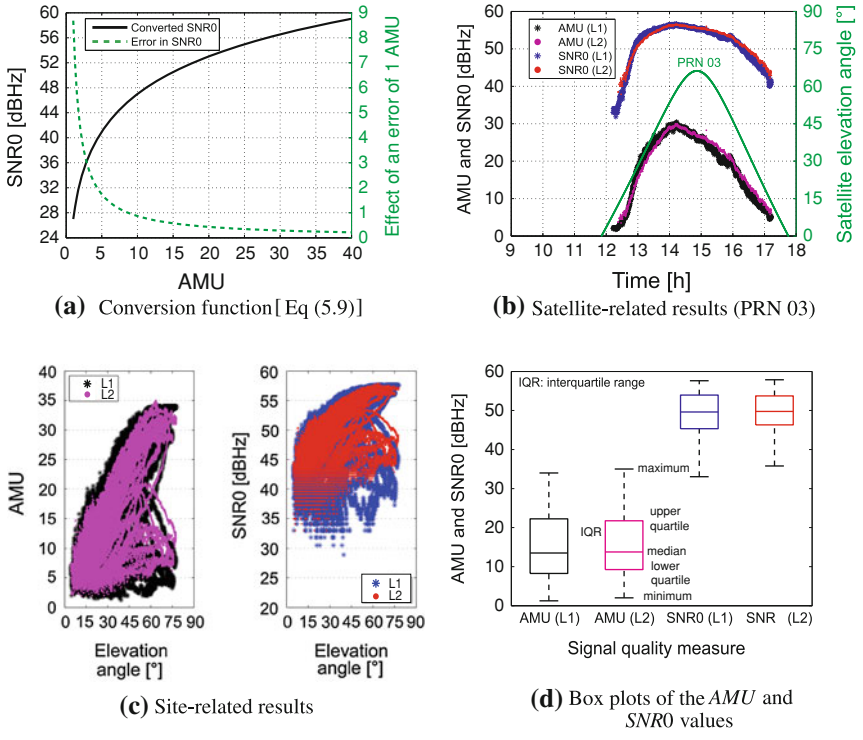


**(a)** Conversion function [ Eq (5.9)] **(b)** Satellite-related results (PRN 03)

**(c)** Site-related results **(d)** Box plots of the *AMU* and *SNR*0 values

**Fig. 5.2** Examples of *AMU* and converted *SNR*0 values in dBHz (site: SPR1, strong multipath, receiver: Trimble 4000SSI, antenna: Trimble 4000ST L1/L2 GEO; Mayer 2006, p. 44)

file. The conversion from *AMU* into *SNR*0 causes an obvious offset and a slight compression of the variation range. In spite of the strong correlation between the signal quality measure and the satellite elevation angle, the maximum *AMU* (or *SNR*0) is reached not at the maximum elevation angle of about 66°, but at about 50°. This coincides with the variation pattern of the received signal power and implies the unrealistic assumption generally made by elevation-dependent weighting models, namely, the larger the satellite elevation angle, the better the observation quality, and the smaller the observation variance. Regarding the items listed in Table 5.1 under "Signal characterisation", this assumption is true for path loss, atmospheric loss and receiver antenna gain, but not valid for satellite antenna gain. Considering all observed satellites, Fig. 5.2c plots the original *AMU* and the converted *SNR*0 versus satellite elevation angle. The offset and compression effects observed in Fig. 5.2b are clearly visible. The large dispersion in signal quality, especially for $e > 50°$, is attributed to the near-ground installation of the GPS antenna (Mayer 2006, p. 45). The box plots shown in Fig. 5.2d provide an excellent illustration of the changes due to the conversion from *AMU* into *SNR*0, namely the increased medians and decreased IQR.

Provided that SNR can be accurately recovered by the receiver, it turns out to be a more realistic quality indicator for GPS observations than the satellite elevation angle. However, due to receiver firmware problems, sudden drops in SNR may occur for high-elevation satellites, even when regarding the same receiver type (Satirapod and Wang 2000). Figure 5.3 illustrates this problem using *AMU* values from the same satellite, which is simultaneously observed at three sites that have different multipath effects, but the same antenna-receiver combination. In this example, obvious sudden drops are present in the PRA1- and OHG1-related *AMU* values, while they are completely absent for the site SPR1 using the same antenna-receiver combination, but with a different firmware version. This emphasises the importance of the information about firmware updates when performing SNR-based data analyses. Furthermore, the site-specific *AMU* presentation in Fig. 5.3c corresponds to the multipath specification provided by Mayer (2006, p. 44), indicating the great potential of SNR in multipath modelling.

## 5.2 Review of Previous Work

Although the potential merits of using signal quality measures as a weighting scheme were outlined by Talbot (1988), it appears that more intensive investigations and comprehensive applications of this quality indicator for GPS phase observations have only been carried out after Langley (1997) published a direct relationship between the phase variance $\sigma^2_{\Phi_i}$ in $m^2$ and the signal-to-noise power density ratio $SNR0_i$ in dBHz as

$$\sigma^2_{\Phi_i} = B_L \cdot \left(\frac{\lambda_i}{2\pi}\right)^2 \cdot 10^{-\left(\frac{SNR0_i}{10}\right)} = C_i \cdot 10^{-\left(\frac{SNR0_i}{10}\right)}, \tag{5.10}$$

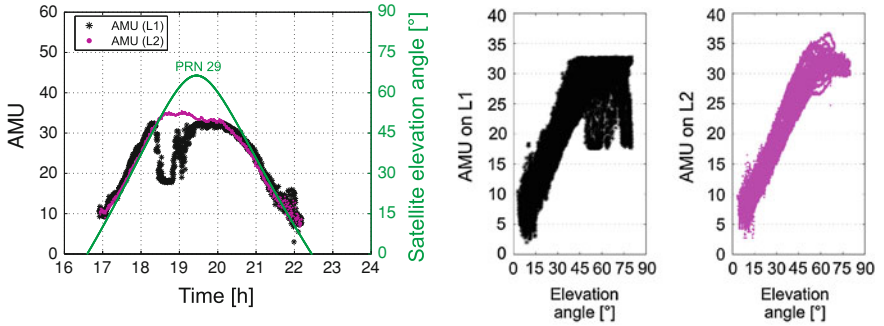


**(a)** Site: PRA1, weak multipath, firmware version: NP 7.24/SP 3.07

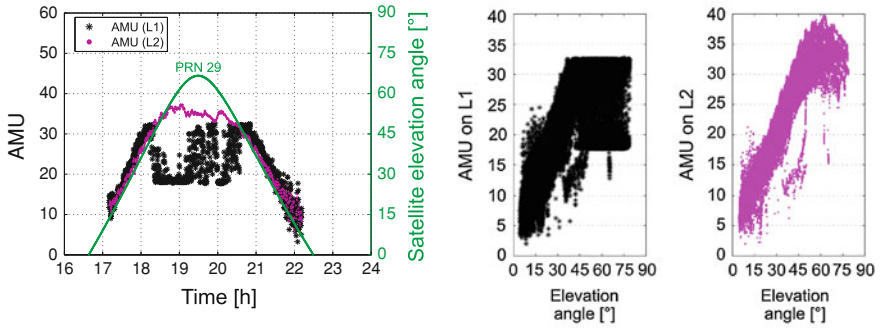


**(b)** Site: OHG1, weak multipath, firmware version: NP 7.24/SP 3.07

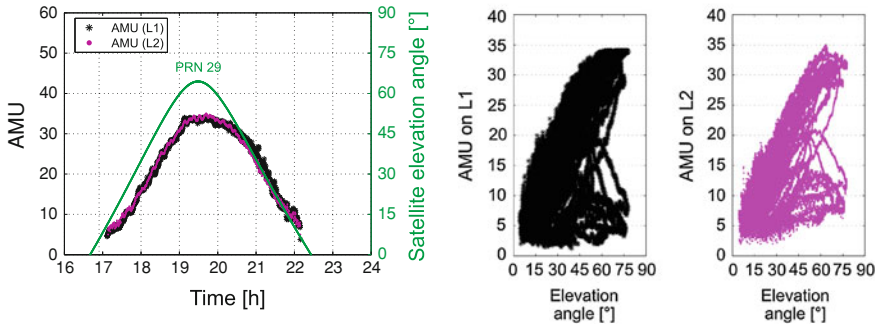


**(c)** Site: SPR1, strong multipath, firmware version: NP 7.09/SP 3.03

**Fig. 5.3** Comparison of satellite- and site-related *AMU* values with respect to multipath impact and receiver firmware (satellite: PRN 29, receiver: Trimble 4000SSI, antenna: Trimble 4000ST L1/L2 GEO, site multipath specification: Mayer 2006, p. 44)

where the subscript $i$ denotes the carrier frequency (e.g., $i = 1$ for L1). The factor $C_i$ in $m^2Hz$ depends on the carrier tracking loop bandwidth $B_L$ in Hz and a quadratic term which is related to the wavelength $\lambda_i$ in m. Using representative loop bandwidths of 5, 10 and 15 Hz for GPS (Braasch and van Dierendonck 1999), Fig. 5.4 depicts the phase standard deviation $\sigma_{\Phi_i}$ derived by means of Eq. (5.10). In the case that

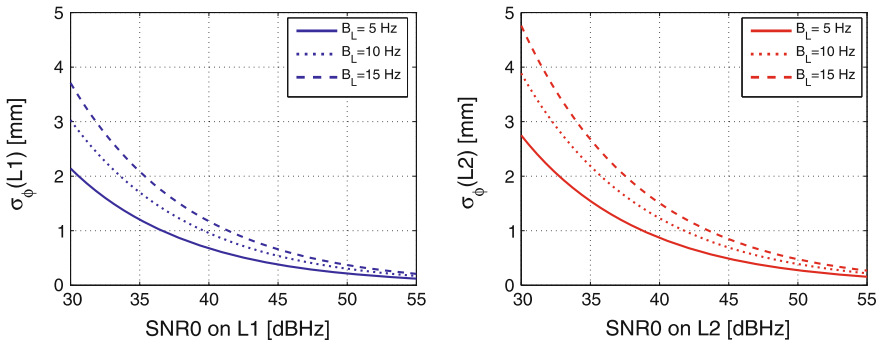


**Fig. 5.4** Illustration of the phase standard deviations derived by means of the SNR-based variance Eq. (5.10) (*left*: L1 with $\lambda_1 = 19.0$ cm, *right*: L2 with $\lambda_2 = 24.4$ cm; see Table 3.2)

$B_L = 15$ Hz, the L1 (L2) phase standard deviation decreases from 3.7 (4.7) to about 0.2 mm as $SNR0$ increases from 30 to 55 dBHz. Furthermore, it can be seen that the phase error is inversely proportional to signal strength and directly proportional to the loop bandwidth and wavelength.

Analysing Eq. (5.10) and Fig. 5.4, one may attempt to improve the noise performance by narrowing the loop bandwidth. However, $B_L$ must be wide enough to be able to follow the receiver dynamics. A tracking loop with a narrow bandwidth may have problems dealing with rapid phase variations. For most static applications, a bandwidth of 2 Hz or less can be used to derive the phase variance (Langley 1997). Instead of specifying a typical $B_L$ value, Hartinger and Brunner (1999) developed the SIGMA-$\epsilon$ model, where the factor $C_i$ is determined based on double-difference residual and $SNR0$ variances, depending upon the receiver and antenna types. By analysing multiple data sets, $C_1$ is estimated to be approximately $1.6 \times 10^{-2}$ m$^2$Hz. Experimental studies using baselines of up to about 1 km have showed that by applying appropriate observation weights, the SIGMA-$\epsilon$ model enables the use of low-elevation data with a cut-off angle of 7.5°. This overcomes the problem of poor satellite geometry and improves the performance of parameter estimation. To illustrate the differences between the commonly used elevation-dependent and SNR-based variance models, i.e., $\sigma_i^2 / \sin^2(e)$ and Eq. (5.10), respectively, Fig. 5.5 compares the phase standard deviations $\sigma_{\Phi_i}$ and observation weights $w_{\Phi_i}$ computed using the elevation angles and $SNR0$ values shown in Fig. 5.1a. Thereby, $\sigma_1$ and $\sigma_2$ are equal to 1 and 1.3 mm, respectively (Dach et al. 2007, p. 144). The frequency-related $C_i$ is calculated in such a way that $\sigma_{\Phi_i} = \sigma_i$ holds for the best observation with the maximum $SNR0_i$ (here 51 dBHz).

As Fig. 5.5a and c show, for L1 observations at satellite elevation angles above 5°, both variance models coincide fairly well in this example. The elevation-dependent weights are obviously equal to $\sin^2(e)$, while the SNR-based ones are computed using $\sigma_i^2 / \sigma_{\Phi_i}^2$. Considering low-elevation observations, for example, at an elevation angle of 3°, the SNR-based phase standard deviations $\sigma_{\Phi_1}$ vary between 4 and 9 mm, while the elevation-dependent ones amount to about 2 cm. As the elevation angle

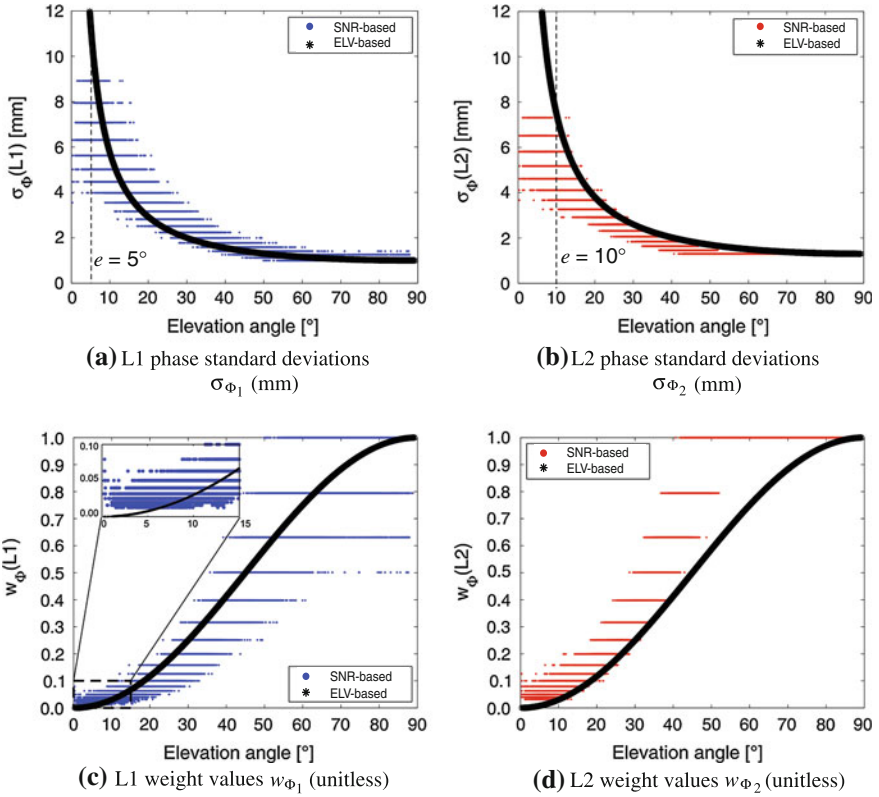


**(a)** L1 phase standard deviations $\sigma_{\Phi_1}$ (mm)

**(b)** L2 phase standard deviations $\sigma_{\Phi_2}$ (mm)

**(c)** L1 weight values $w_{\Phi_1}$ (unitless)

**(d)** L2 weight values $w_{\Phi_2}$ (unitless)

**Fig. 5.5** Phase standard deviations and observation weights derived using the elevation-dependent $[\sigma_i^2 / \sin^2(e)]$ and SNR-based [Eq. (5.10)] variance models ($\sigma_1 = 1$ mm, $\sigma_2 = 1.3$ mm, $SNR0_i$ from Fig. 5.1, $C_1 \approx 0.126$ m$^2$Hz, $C_2 \approx 0.213$ m$^2$Hz, $w_{\Phi_i} = \sigma_i^2 / \sigma_{\Phi_i}^2$)

further decreases, $\sigma_{\Phi_1}$ increases rapidly to about 6 cm for $e = 1°$. In contrast to L1, the elevation-dependent variance model appears to be incapable of realistically characterising the observation quality on L2. Throughout the whole range of elevation angles, particularly for $e < 10°$, it provides considerably larger $\sigma_{\Phi_2}$ (see Fig. 5.5b) and smaller $w_{\Phi_2}$ (see Fig. 5.5d) than the SNR-based approach, indicating an underestimation of the L2 observations in the LS parameter adjustment. Moreover, this model comparison produces an important message that a frequency-related observation weighting is possible when using signal quality measures instead of the satellite elevation angle. In fact, only considering parameter estimates, it is not even necessary to choose a suitable receiver bandwidth $B_L$ or to estimate a realistic model parameter $C_i$, since the term $C_i$ only changes the a priori variance factor (Collins and Langley 1999, p. 26). Nevertheless, in the interest of quality control, parameter constraining and relative weighting of observation groups, $B_L$ and $C_i$ should be carefully specified.

Although the variance model given by Eq. (5.10) allows for a more realistic quality assessment of GPS observations, it ignores any contribution to the phase noise from

the local oscillator and is only suitable for relatively strong signals well above the tracking threshold of the receiver (Collins and Langley 1999, p. 4). However, under real observational conditions, signal distortions occur, for example, due to multipath and diffraction. To achieve a realistic SNR-based error characterisation of GPS phase observations without the a priori knowledge about the receiver environment, Brunner et al. (1999) developed the SIGMA-$\Delta$ model that automatically computes the phase noise based on the measured *SNR*0 and a *SNR*0 template for a certain antenna type. Such a template is defined by the highest *SNR*0 value at a certain satellite elevation angle. Applying the SIGMA-$\Delta$ model in static and kinematic GPS surveys, the position errors caused by signal diffraction can be reduced by about 50–85 %.

Wieser and Brunner (2000) verified the effectiveness of estimating the actual phase observation noise in the SIGMA-$\epsilon$ model, as well as the appropriateness of using SNR as an indicator for signal distortions in the SIGMA-$\Delta$ model. In addition, the limitations of the SNR-based weighting schemes were demonstrated, particularly in the presence of strong multipath effects. To overcome these limitations, the SIGMA-$\epsilon$ model was extended by applying robust estimation methods (e.g., the Danish method) and by incorporating residual information into multipath and diffraction handling. The extended weighting model showed good performance in identifying and removing biases, where its efficiency mainly depends on the redundancy of the observation data and the evaluation of the residual covariance matrix. In this context, the epoch-wise data analysis strategy, commonly implemented in GPS processing software, is questionable. If all epochs are processed simultaneously, the temporal (inter-epoch) correlations must be taken into account. Satirapod and Wang (2000) compared the two quality indicators, SNR and satellite elevation angle, and concluded that SNR generally represents a more realistic quality measure, but both of them do not always reflect reality.

In order to mitigate multipath and interference in GPS relative positioning in engineering surveying, Lau and Mok (1999) suggested the CALMS (combined AFM and LSM method with SNR weighting) approach, which combines the ambiguity function method (AFM; Mader 1992) and the SNR-weighted least-squares method (LSM). Thereby, the double-difference weight matrix is multiplied by a SNR cofactor matrix, resulting in the final weight matrix for the LS adjustment. Employing this SNR-weighted LS algorithm in short-baseline ($<10$ km) applications, improved positioning accuracy was reported when using 1 min of GPS data (6 epochs) collected in a strong multipath environment. Since the multipath error is reduced by means of an advanced stochastic model, a long observation period for averaging out multipath is not required.

Taking advantage of other favourable properties of SNR, for instance, being sensitive to carrier-phase multipath and reflecting changes in the multipath environment, Bilich and Larson (2007) developed a method to map the temporally variable amplitude and frequency content of various multipath constituents by applying the continuous wavelet transform (see Sect. 2.4.2) to SNR time series. Using representative continuously operating GPS sites from geodetic networks, it was concluded that near-field multipath, associated with high satellite elevation angles, does not significantly contribute to position errors, while the impact of far-field multipath, particularly that

caused by topographic features, seems to be more serious than previously believed. If multipath signals are not correctly understood and sufficiently modelled, they may be mistaken for seismic waves in applications of GPS seismology. Based on the theory that the time-evolving property of multipath leads to equal-frequency, but out-of-phase oscillations in carrier-phase and SNR, Bilich et al. (2008) proposed the combined wavelet-ALS algorithm for modelling GPS phase multipath error. The model parameters, such as the amplitude and relative phase, are estimated by means of an adaptive LS (ALS) method. Applying this approach to short-baseline (11–17 m) network solutions using GPS data collected from a large salt flat (Salar de Uyuni), multipath signals with periods between 200 and 2,000 s can be successfully detected and sufficiently reduced. It was shown that a reduction in phase residual noise of up to 20 % is achievable for static positioning, and an improvement of 1–7 dB in spectral power at multipath periods is possible for kinematic positioning. In spite of the considerable enhancements, the suggested algorithm still has difficulties in extracting multipath amplitude and phase information from SNR time series, and is restricted to simple multipath environments.

According to the same relationship between carrier-phase multipath error and SNR, Rost and Wanninger (2009) derived a simplified multipath correction model for GPS static positioning and single dominant reflectors. It requires a SNR resolution of at least 0.25 dBHz and mainly considers the multipath relative phase as well as the ratio of the composite and direct signal amplitudes. Using GPS data from a short baseline of 10 m, established on a parking lot, it was verified that the SNR-based multipath corrections only depend on the receiver antenna height and satellite elevation angle due to the large horizontal reflector. Applying the correction values to the phase observations, both the double-difference residuals and single-epoch coordinate estimates are improved by almost 25 %. In Rost and Wanninger (2010), this model was used to correct the GNSS (GPS/GLONASS) data from the continuously operating reference stations (CORS) of the German SA*POS*® sub-network of Saxony-Anhalt. Comparing the LC3 single-epoch coordinate standard deviation before and after applying the multipath corrections, both amelioration of up to 13 % and deterioration of up to −6.5 % are observed in the height and horizontal components, respectively. If the model assumption of one well-defined horizontal reflector is fulfilled, a large portion of the phase multipath effects can be removed. Nonetheless, the proposed method is not generally applicable to multipath mitigation.

Enabling a more realistic assessment of GPS observation quality, SNR-based variance (or weighting) models are preferable for GPS data analysis, particularly when including observations from low-elevation satellites. However, the performance of the variance model given by Eq. (5.10) strongly depends on how well the generally unknown loop bandwidth $B_L$ is specified. Furthermore, as mentioned above, such a variance model ignores the contribution of the local oscillator to the phase noise. By individually estimating the factor $C_i$ for different antenna and receiver types, the SIGMA-$\epsilon$ model is capable of considering site-specific environments and antenna-receiver characteristics. Nevertheless, it still has the disadvantage of being only strictly suitable for relatively strong signals well above the tracking threshold of the receiver (Collins and Langley 1999, p. 4). To overcome these drawbacks

of this analytical SNR-based variance model, an empirical SNR-based weighting scheme is developed in this thesis, which also accounts for site-specific effects and antenna-receiver characteristics. Due to the unrealistic assumptions of the SNR-based multipath modelling (e.g., a well-defined horizontal reflector), the sidereal stacking technique is employed in this work, which makes use of multiple consecutive days of residual time series (see Sect. 7.2.5).

## 5.3 SNR-Based Weighting Model

In this section, an empirical SNR-based weighting model is presented. Following a detailed description of its realisation and contribution to the GPS stochastic model, its advantages are demonstrated in comparison to other analytical and empirical approaches using SNR or the satellite elevation angle. Next, the model implementation in the Bernese GPS Software 5.0 is briefly discussed. Finally, the key properties of the proposed SNR-based weighting scheme are summarised considering different aspects, emphasising its strengths in GPS data analysis.

### *5.3.1 Model Realisation*

The empirical SNR-based weighting model relies upon a simple and intuitive principle that the best GPS observations with the largest SNR should obtain the maximum weight of one. The weights for other measurements depend on the minimum-related ratios of the corresponding SNR values to the maximum SNR. To ensure the comparability between various SNR realisations (see Sect. 5.1), the signal quality measures should be available as $SNR0$ in dBHz or can be converted into $SNR0$, where external information from receiver manufacturers, such as SNR unit and computation, may be necessary. Using observation data in the RINEX format, for example, Version 2.10, SNR measurements are reported as observable types S1 and S2, and represent the raw signal strengths as provided by the receiver for L1 and L2 phase observations (Gurtner 2002, Sect. 0.4). The current RINEX Version 3.00 requires that the raw signal strengths should be stored in dBHz if possible, where the raw SNR values are obtained at the correlator output without attempting to recover any correlation loss. In addition, a new header record `SIGNAL STRENGTH UNIT` is available, providing the unit of the signal quality measurements (Gurtner and Estey 2007, pp. 10, 28). The raw signal strength in dBHz can be expressed as a scale of 1–9 (1: very weak, . . . , 9: very strong) by means of

$$SNR_{rnx} = \min\{\max\left[\mathrm{INT}(SNR0/6), 1\right], 9\}, \tag{5.11}$$

resulting in the so-called RINEX signal strength indicator (Gurtner and Estey 2007, Sect. 5.7). A $SNR_{rnx}$ of 5 corresponds to a $SNR0$ of about 35 dBHz and is the threshold for average signal quality. If $SNR_{rnx}$ is equal to zero, the associated $SNR0$ is unknown

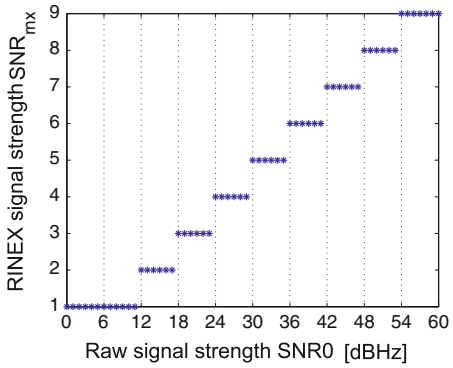


| SNR0 [dBHz] | SNRrnx |
|---|---|
| < 12 | 1 |
| 12-17 | 2 |
| 18-23 | 3 |
| 24-29 | 4 |
| 30-35 | 5 |
| 36-41 | 6 |
| 42-47 | 7 |
| 48-53 | 8 |
| ≥ 54 | 9 |

**Fig. 5.6** Projection of the raw signal strength *SNR*0 in dBHz into the RINEX signal strength indicator $SNR_{rnx}$ [Gurtner and Estey 2007, Table 7; see Eq. (5.11)]

or not present. Figure 5.6 shows the SNR projection given by Eq. (5.11) in graphic and tabular form. As the graph displays, the transform from *SNR*0 into $SNR_{rnx}$ can be considered linear.

Although signal quality data can be stored in the unique unit dBHz, differences in *SNR*0 are still present due to receiver characteristics (e.g., hardware, receiver firmware) and site-specific effects (e.g., multipath). The corresponding variations in observation quality should be considered in the SNR-based weighting model to achieve a more realistic noise assessment of GPS phase measurements. Keeping this in mind, an empirical SNR-based weighting scheme is realised in two steps, schematically shown in Fig. 5.7 for GPS relative positioning.

In the first step, signal quality measurements are extracted from the RINEX observation files, where missing SNR data are marked by zero. As an alternative to the self-programmed routine, SNR values can be conveniently obtained for each satellite by applying the `cf2ps` program (Hilla 2002) to the TEQC plot files (Estey and Meertens 1999). If the extracted SNR quantities are not *SNR*0 in dBHz (e.g., AMU, *SNR* in dB), they are converted into *SNR*0 based on the information provided by receiver manufacturers. Once the SNR data are aligned to a comparable level, for each antenna-receiver combination (ARC) being present in the network, the frequency-dependent minimum and maximum *SNR*0 values, denoted as $SNR0^{\min}_{ARC,i}$ and $SNR0^{\max}_{ARC,i}$, respectively, are searched over the entire observation period. This procedure guarantees that the found extreme signal strengths are representative with respect to the site's environments, atmospheric variations as well as antenna and receiver characteristics. The zero-valued SNR data due to missing observations are excluded from the minimum search procedure. In order to avoid the situation where the found global extremes are actually outliers, for each ARC, statistical analysis of *SNR*0 is performed by means of box plots, as demonstrated in Fig. 5.1b.

Following the first step in which the SNR measurements are homogenised and the global references for low- and high-quality observations are found, the second step produces individual weights for each L1 and L2 phase observation by calculating the

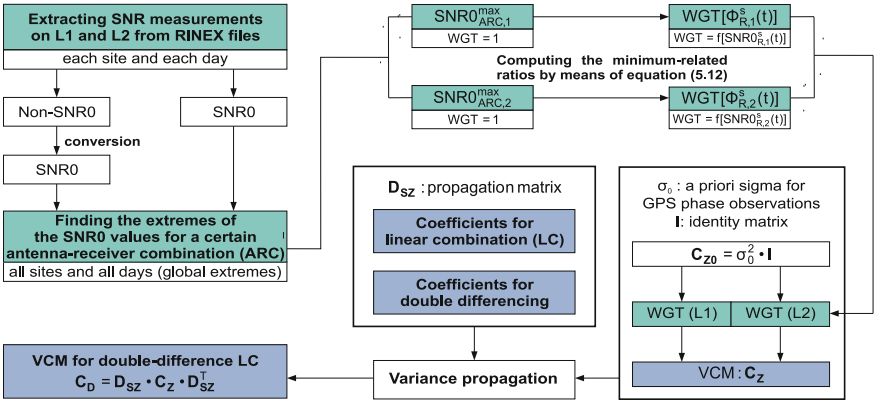


**Fig. 5.7** An empirical SNR-based observation weighting scheme and its contribution to the stochastic model in GPS relative positioning (WGT: weight, VCM: variance-covariance matrix), after Luo et al. (2008a,b)

minimum-related ratio between the actual *SNR*0 and the corresponding maximum. Considering the phase observation $\Phi^s_{R,i}(t)$, which is related to receiver $R$, satellite $s$, frequency $i$ and epoch $t$, the corresponding SNR-based weight is computed as

$$w\left[\Phi^s_{R,i}(t)\right] = f\left[SNR0^s_{R,i}(t)\right] = \left[a + (1-a)\cdot\left(\frac{SNR0^s_{R,i}(t) - SNR0^{\min}_{ARC,i}}{SNR0^{\max}_{ARC,i} - SNR0^{\min}_{ARC,i}}\right)\right]^2, \tag{5.12}$$

where the parameter $a$ is introduced to avoid the singularity problem of the cofactor $q = w^{-1}$ in the case that $SNR0^s_{R,i}(t) = SNR0^{\min}_{ARC,i}$. To fulfil the precondition $f(SNR0^{\max}_{ARC,i}) = 1$, a factor of $(1-a)$ is multiplied to the minimum-related ratio. For representative *SNR*0 values between 10 and 55 dBHz (see Fig. 5.6), Fig. 5.8 illustrates the weights and cofactors derived from Eq. (5.12) using different specifications for $a$. As $a$ decreases from 0.1 to 0.01, one can discern an overall downweighting effect, with decreased weights and increased cofactors, particularly for low-quality signals. By considering Fig. 5.5a and c, $a = \sin 5^\circ \approx 0.1$ is used in this thesis to reduce the downweighting effect on low-quality observations of weak signals.

The SNR-based weights computed using Eq. (5.12) improve the scaled identity matrix, which is denoted as $\boldsymbol{C_{Z0}}$ in Fig. 5.7, to the variance-covariance matrix (VCM) $\boldsymbol{C_Z}$ with different diagonal elements. Next, $\boldsymbol{C_Z}$, the VCM of zero-differences, is propagated by considering the propagation matrix $\boldsymbol{D_{SZ}}$, which contains the coefficients for linear combination and double differencing (see Fig. 3.6). The resulting VCM of double-differences $\boldsymbol{C_D}$ is then used for the LS parameter estimation. Although in this thesis the empirical SNR-based weighting model is only applied to GPS relative positioning, it can be easily adapted to precise point positioning (PPP) by neglecting the variance propagation step with respect to double differencing.

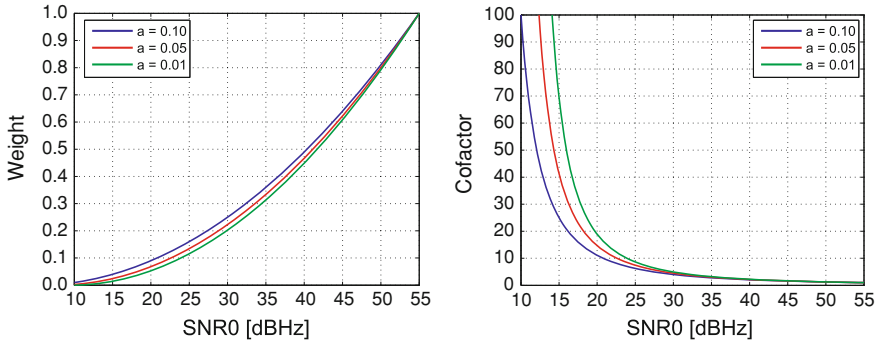


**Fig. 5.8** Influence of the model parameter $a$ in Eq. (5.12) on the SNR-based weight and cofactor values ($SNR0^{\min}_{ARC,i} = 10$ dBHz, $SNR0^{\max}_{ARC,i} = 55$ dBHz)

### *5.3.2 Model Comparison*

In this section, the suggested SNR-based weighting model (EMPSNR2) is compared with different alternatives, such as the analytical approach (ANLSNR) given by Eq. (5.10), another empirical method (EMPSNR1) proposed by Mayer (2006, p. 62) and the commonly used elevation-dependent weighing function $\sin^2(e)$ denoted as CSC2(BS) in Fig. 3.3.

For $SNR0$ varying from 10 and 35 to 55 dBHz, Fig. 5.9 compares the weight and cofactor values produced by ANLSNR and EMPSNR2, where the ANLSNR-related weights are computed with respect to the maximum $SNR0$. As Collins and Langley (1999, p. 4) noted, the analytical model ANLSNR is only suitable for relatively strong signals (i.e., $SNR0 > 35$ dBHz), while the empirical approach EMPSNR2 is also able to deliver reasonable weights for relatively weak signals (i.e., $SNR0 \leq 35$ dBHz). This indicates a better performance of EMPSNR2 for both low- and high-quality GPS measurements. Furthermore, when decreasing the $SNR0$ range from [10, 55] to [35, 55], the differences between ANLSNR and EMPSNR2 also decrease.

Analysing GPS data from the densification network of the Antarctic Peninsula, Mayer (2006, Sect. 5.4.2) computed SNR-based observation weights empirically by simply dividing the signal quality measurements by the maximum found during an observation campaign. This approach assumes a homogenous antenna-receiver combination within a survey campaign and delivers almost azimuth-independent weights between 0.1 and 0.3 for low-elevation (i.e., $e < 20°$) data. For GPS measurements from medium- and high-elevation satellites, the corresponding weights are generally larger than 0.5 (Mayer 2006, pp. 62, 67). Figure 5.10 illustrates the weights and cofactors produced by EMPSNR1 and EMPSNR2. From Fig. 5.10, one can easily discern that EMPSNR1 always produces larger weights than EMPSNR2, particularly for the narrower $SNR0$ variation range [35, 55]. Overweighting low-quality observations leads to small cofactor values and overestimates the contribution of low-quality data to the LS parameter estimation.

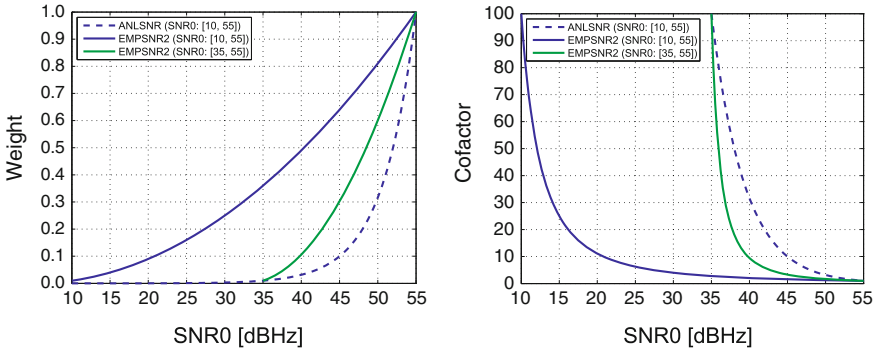


**Fig. 5.9** Comparison of the weight and cofactor values produced by the observation weighting models ANLSNR and EMPSNR2 [ANLSNR: $w_{\Phi_i} = \sigma^2_{\Phi_i}(SNR0_i^{\max} = 55\,\text{dBHz})/\sigma^2_{\Phi_i}(SNR0_i)$, see Eq. (5.10); EMPSNR2: $a = 0.1$, see Eq. (5.12)]

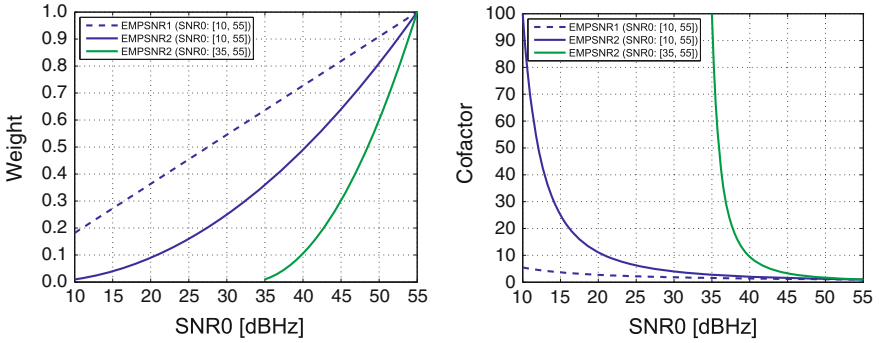


**Fig. 5.10** Comparison of the weight and cofactor values produced by the empirical observation weighting models EMPSNR1 and EMPSNR2 [EMPSNR1: $w_{\Phi_i} = SNR0_i/SNR0_i^{\max}$, Mayer 2006, Sect. 5.4.2; EMPSNR2: $a = 0.1$, see Eq. (5.12)]

Taking the $SNR0$ data shown in Fig. 5.1a as an example, Fig. 5.11 compares the empirically derived observation weights depending on the satellite elevation angle. If EMPSNR1 is applied, observations at $e < 20°$ already maintain considerably large weights of about 0.7, which attenuates the qualitative difference between an average and a good observation. This kind of overweighting effect is considerably reduced by means of the proposed EMPSNR2. Thereby, low-elevation observations obtain more realistic weights of up to about 0.4. Therefore, the employment of EMPSNR2 seems to achieve a balance between appropriately downweighting low-quality observations and effectively improving the satellite geometry by incorporating low-elevation measurements into the parameter adjustment.

The commonly used elevation-dependent variance models presented in Table 3.6 depend on the cosecant function of the satellite elevation angle, i.e., $1/\sin(e)$, which actually represents a first-order approximation of the tropospheric mapping function.

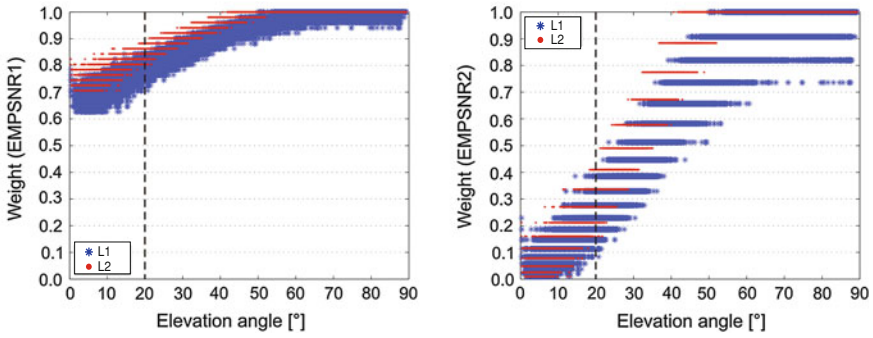


**(a)** Weighting model: EMPSNR1 **(b)** Weighting model: EMPSNR2

**Fig. 5.11** Empirical weights derived using the *SNR*0 measurements shown in Fig. 5.1a

The underlying theory is that the tropospheric delay error increases towards the horizon, as does the amount of noise inherent to GPS observations. Therefore, the variance of phase noise is assumed to be directly proportional to the squared value of $1/\sin(e)$ (Collins and Langley 1999, p. 1). Figure 5.12 compares the empirical SNR-based weighting model EMPSNR2 with the elevation-dependent weighting scheme CSC2(BS) (i.e., $\sin^2(e)$; Dach et al. 2007, p. 144) with respect to observation data volume, antenna-receiver combination and site-specific multipath impact.

Comparing the weight values for the site RAVE on a daily basis, Fig. 5.12a shows the advantage of EMPSNR2 in attenuating observation downweighting effects over the whole elevation range. Moreover, the differences in observation quality between L1 and L2 become more obvious for $e > 20°$, and they cannot be accounted for by means of CSC2(BS), but by applying EMPSNR2 (see also Fig. 5.11b). In this example, the *SNR*0 values on the L2 carrier frequency range from 36 to 51 dBHz and are well above the tracking threshold of 35 dBHz (see Figs. 5.1b and 5.6). Accordingly, similar results are also obtained using the analytical approach ANLSNR (see Figs. 5.5d and 5.9).

In addition to long-term (24 h) GPS measurements, short-term static observations are also used for model comparison. Although the weight values presented in Fig. 5.12b–d are related to a 1 h time interval, the antenna-receiver-specific *SNR*0 extremes are determined based on representative data sets. Despite the different data volumes and receiver firmware versions, the variation patterns of the SNR-based weights shown in Fig. 5.12b are quite similar to those displayed in Fig. 5.12a. This demonstrates the potential of EMPSNR2 in short-term static applications if reliable *SNR*0 extremes are available, for example, in the case of CORS.

For the same observation period, a similar degree of multipath impact, but another antenna-receiver combination, Fig. 5.12c illustrates SNR-based weights with considerably different patterns when compared to Fig. 5.12b. The antenna-receiver-specific handling, which is realised in EMPSNR2, contributes to the maintenance of instrumental characteristics, although both the Leica and Trimble receivers deliver *SNR*0

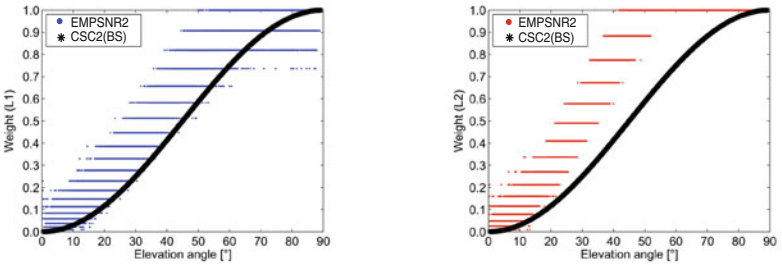


**(a)** Site: RAVE, weak multipath, 24 h observation data, sampling interval: 15 s, receiver: Leica SR520, antenna: LEIAT503, firmware version: 4.01

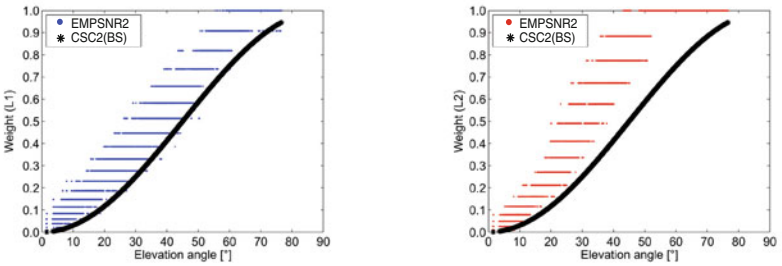


**(b)** Site: RAVE, weak multipath, 1 h observation data, sampling interval: 1 s, receiver: Leica SR520, antenna: LEIAT503, firmware version: 4.1

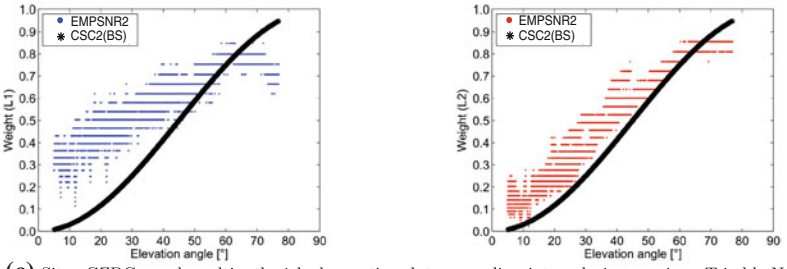


**(c)** Site: GZBG, weak multipath, 1 h observation data, sampling interval: 1 s, receiver: Trimble NetR5, antenna: TRM55971.00 TZGD, firmware version: Nav 3.20/Boot 3.10

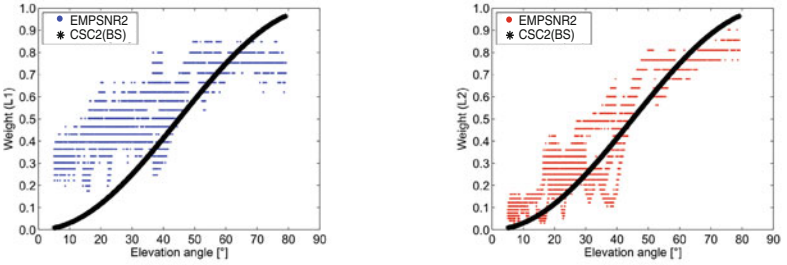


**(d)** Site: DARM, strong multipath, 1 h observation data, sampling interval: 1 s, receiver: Trimble NetR5, antenna: TRM55971.00 TZGD, firmware version: Nav 3.30/Boot 3.10

**Fig. 5.12** Comparison of the observation weights produced by CSC2(BS) and EMPSNR2 considering different aspects (**a** DOY2004:186, **b–d** DOY2007:161, 17–18 h, GPS time)

in dBHz (Landau 2006). Furthermore, the elevation-dependent weighting model CSC2(BS) seems to produce more serious downweighting effect on the L1 (L2) observations from the Trimble (Leica) receiver at low (high) elevation angles. In Fig. 5.12d, the SNR-based and elevation-dependent weights are compared for the site DARM, which has the same antenna-receiver combination as the site GZBG, but a stronger multipath impact (see Fig. 4.6c). This can be well captured by means of EMPSNR2 due to the fact that the frequency and amplitude content of SNR data are directly related to carrier-phase multipath errors (Bilich et al. 2008).

Another advantage of EMPSNR2 over CSC2(BS) is that SNR measurements respond to environmental variations, while GPS satellite elevation angles observed at the same site repeat with an approximate period of one mean sidereal day. As a result, SNR-based weights reflect changes in observation quality induced by variable atmospheric conditions, while elevation-dependent weights completely ignore these day-to-day variations and thus produce an unrealistic mapping of observation quality. To demonstrate this benefit from EMPSNR2, Fig. 5.13 takes the site DARM as an example and compares the 1 h L2 weights on three consecutive days (DOY2007:179–181). By considering an approximate repeat time of the GPS constellation of one mean sidereal day (i.e., 23 h 56 min 4 s; see Sect. 7.2.5), the observation weights are determined under an almost identical satellite geometry, as illustrated in Fig. 5.13a.

For elevation angles around 20° as well as between 50 and 70°, Fig. 5.13b and d exhibit minor, but visible differences in the L2 weights between days 179 and 181. On day 180, large variations are present, particularly at high elevation angles (see Fig. 5.13c). Taking the strong multipath environment of the site DARM into account, these day-to-day variations may be attributed to the changes in site reflection properties, which are caused by variable atmospheric conditions (see *RH* at FRAN in Fig. 4.8c). In contrast, due to the repeating satellite geometry, the elevation-dependent weights are identical on different days.

The above comparison emphasises the advantages of the proposed SNR-based weighting scheme EMPSNR2 in downweighting reduction, overweighting prevention and realistic characterisation of GPS observation quality. In order to exploit these benefits in GPS data analysis and to improve the performance of parameter estimation, the EMPSNR2 model is experimentally implemented in the Bernese GPS Software 5.0 (Dach et al. 2007).

### *5.3.3 Model Implementation*

The implementation of the empirical SNR-based weighting model consists of two parts, namely weight calculation and weight application, schematically shown in Fig. 5.14. According to the flowchart presented in Fig. 5.7, the computation of the frequency-related weights is performed in MATLAB. As a result, for each site in each session, a weight file (`WGT`) is generated, which contains epochs in GPS time, satellite PRN (pseudo random noise) numbers and observation weights for L1 and L2

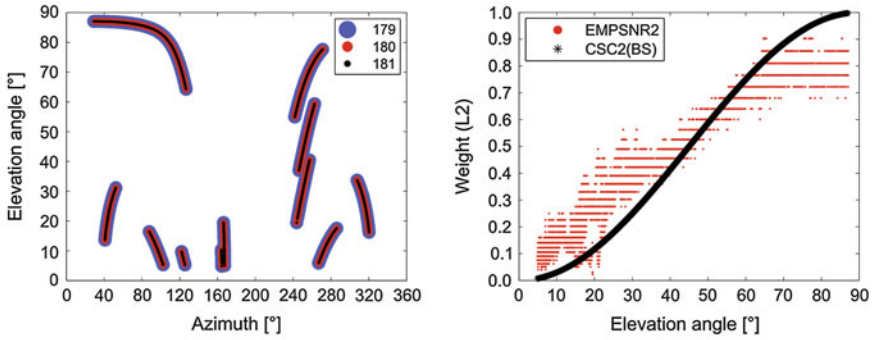


**(a)** Repeating satellite geometry **(b)** Weight values on day 179

**(c)** Weight values on day 180 **(d)** Weight values on day 181

**Fig. 5.13** Comparison of the 1 h L2 observation weights produced by CSC2(BS) and EMPSNR2 under an almost identical satellite geometry on three consecutive days (site: DARM, strong multipath, DOY2007:179–181, 17–18 h, GPS time, sampling interval: 1 s)

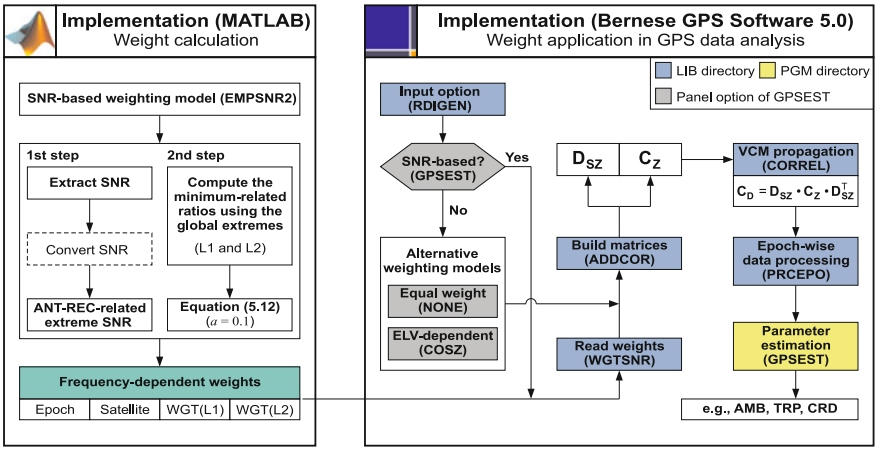


**Fig. 5.14** Implementation of EMPSNR2 in the Bernese GPS Software 5.0 for relative positioning

phase measurements. The WGT files are located in an additional campaign directory named as SNR (i.e., ${P}/MYCAMP/SNR/*.WGT).

At the preliminary stage of the implementation of EMPSNR2 in the Bernese GPS Software 5.0, the input panel of the main program GPSEST, located in the user-specific directory (${U}/PAN/GPSEST.INP), is modified by adding another observation weighting option SNR to the already existing models NONE (i.e., equal weight with $w = 1$) and COSZ (i.e., elevation-dependent weight with $w = \sin^2(e)$). To connect the extended weighting option to the related Fortran routines, a new keyValue must be specified in the subroutine RDIGEN, which is located in the library directory (${C}/LIB) and has the task of reading general input options for GPSEST (${C}/PGM). If the SNR-based weighting model is chosen for parameter estimation, observation weights are read from the WGT files by the self-written subroutine WGTSNR, which is also located in the LIB directory. Otherwise, one of the standard weighting models (NONE or COSZ) is applied.

After importing the observation weights, the VCM of zero-differences $\boldsymbol{C_Z}$ is constructed by the subroutine ADDCOR. The building of the propagation matrix $\boldsymbol{D_{SZ}}$ is not affected by a change in the observation weighting model, since its elements only depend on the coefficients for the used linear combination and double differencing (see Fig. 3.6). Once $\boldsymbol{C_Z}$ and $\boldsymbol{D_{SZ}}$ are available, the VCM of double-differences $\boldsymbol{C_D}$ can be derived by applying the variance-covariance propagation law to $\boldsymbol{C_Z}$, which is accomplished by the subroutine CORREL (see Fig. 5.7 for $\boldsymbol{C_Z}$, $\boldsymbol{D_{SZ}}$ and $\boldsymbol{C_D}$). Benefiting from the more realistic SNR-based observation weights, such an advanced stochastic model enhances the epoch-wise data processing performed by the subroutine PRCEPO. The main program GPSEST calls PRCEPO and estimates the unknown parameters, such as phase ambiguities (AMB), site-specific troposphere parameters (TRP) and station coordinates (CRD). Improvements in the parameter estimates will reflect the superior performance of the proposed SNR-based weighing model in comparison to the standard elevation-dependent one.

For the residual-based temporal correlation modelling, which will be presented in Chap. 7, double-difference residuals are saved, along with the corresponding time stamps and information about satellite geometry. The necessary modifications were first made in the Bernese GPS Software 4.2 by Howind (2005) and then adapted to the Version 5.0 by Luo et al. (2007, p. 27).

## 5.4 Concluding Remarks

Being a more realistic quality indicator for GPS phase observations, the signal-to-noise ratio (SNR) holds great potential for improving the stochastic model in GPS data analysis. This chapter introduced an empirical SNR-based weighting model called EMPSNR2, which relies upon a minimum-related scaling of representative signal quality measurements. In view of downweighting effect reduction and realistic quality assessments, EMPSNR2 appears to be superior to the analytical approach ANLSNR proposed by Langley (1997), as well as to the commonly used elevation-

**Table 5.2** Key properties of the elevation-dependent and SNR-based weighting models

| Aspect | CSC2(BS): $\sin^2(e)$ | EMPSNR2: Eq. (5.12) |
|---|---|---|
| Quality indicator | Indirect: satellite elvation angle ($e$) | Direct: signal-to-noise ratio (SNR) |
| Model principle | Squared inverse of the tropospheric mapping function | Antenna-receiver-specific scaling of SNR measurements |
| Application area | Kinematic, short- and long-term static positioning | Short- and long-term static positioning (e.g., CORS[a]) |
| Degree of reality | Low, affected by site-specific effects and variable atmospheric conditions | High, due to the sensitivity of SNR to different quality limiting factors (e.g., multipath) |
| Individual weights for L1 and L2 | Impossible, due to the same satellite elevation angle for both frequencies | Possible, due to the individual SNR registration for each carrier frequency |
| Downweighting | Possible, particularly at low elevation angles | Considerably reduced over the whole elevation range |
| Complexity | Simple, low computational cost | Complex, high computational cost |

[a] CORS: continuously operating reference stations

dependent weighting scheme CSC2(BS) [i.e., $\sin^2(e)$]. In this thesis, EMPSNR2 has been experimentally implemented in the Bernese GPS Software 5.0, and its advantages over CSC2(BS) in GPS relative positioning will be presented in the next chapter. Table 5.2 compares the key properties of CSC2(BS) and EMPSNR2 considering different aspects (Luo et al. 2008a).

## References

Betz, J. (2010). Link budgets. Paper presented at the Meeting of International Committee on GNSS, Working Group A: Compatibility and Interoperability, Turin, Italy, 19 Oct.

Bilich, A., & Larson, K. M. (2007). Mapping the GPS multipath environment using the signal-to-noise ratio (SNR). *Radio Science*, *42*, RS6003. doi:10.1029/2007RS003652.

Bilich, A., Larson, K. M., & Axelrad, P. (2008). Modeling GPS phase multipath with SNR: Case study from the Salar de Uyuni, Boliva. *Journal of Geophysical Research*, *113*, B04401. doi:10.1029/2007JB005194.

Braasch, M. S., & van Dierendonck, A. J. (1999). GPS receiver architectures and measurements. *Proceedings of the IEEE*, *87*(1), 48–64. doi:10.1109/5.736341.

Brunner, F. K., Hartinger, H., & Troyer, L. (1999). GPS signal diffraction modelling: The stochastic SIGMA-Δ model. *Journal of Geodesy*, *73*(5), 259–267. doi:10.1007/s001900050242.

Butsch, F., & Kipka, A. (2004). Die Bedeutung des Signal- zu Rauschleistungsverhältnisses und verwandter Parameter für die Messgenauigkeit bei GPS. *Allgemeine Vermessungs-Nachrichten (AVN)*, *111*(2), 46–55.

Collins, J. P., & Langley, R. B. (1999). Possible weighting schemes for GPS carrier phase observations in the presence of multipath. Department of Geodesy and Geomatics Engineering, Final contract report for the United States Army Corps of Engineers Topographic Engineering Center, No. DAAH04-96-C-0086/TCN 98151, University of New Brunswick (UNB), New Brunswick.

Dach, R., Hugentobler, U., Fridez, P., & Meindl, M. (2007). Bernese GPS Software Version 5.0. Astronomical Institute, University of Bern, Stämpfli Publications AG, Bern.

Estey, L. H., & Meertens, C. M. (1999). TEQC: The multi-purpose toolkit for GPS/GLONASS data. *GPS Solutions*, *3*(1), 42–49. doi:10.1007/PL00012778.

GPS-SPS-SS (1995). Global Positioning System standard positioning service signal specification (2nd ed.). United States Coast Guard, 2 June.

Gurtner, W. (2002). RINEX: The Receiver Independent Exchange Format Version 2.10. Available online at ftp://igscb.jpl.nasa.gov/igscb/data/format/rinex210.txt, accessed on 23 Feb, 2011.

Gurtner, W., & Estey, L. (2007). RINEX: The Receiver Independent Exchange Format Version 3.00. Available online at ftp://ftp.unibe.ch/aiub/rinex/rinex300.pdf, accessed on 23 Feb, 2011.

Hartinger, H., & Brunner, F. K. (1999). Variances of GPS phase observations: The SIGMA-$\epsilon$ model. *GPS Solutions*, *2*(4), 35–43. doi:10.1007/PL00012765.

Hilla, S. (2002). A new plotting program for Windows-based TEQC users. *GPS Solutions*, *6*(3), 196–200. doi:10.1007/s10291-002-0027-1.

Hofmann-Wellenhof, B., Lichtenegger, H., & Wasle, E. (2008). *GNSS-Global Navigation Satellite Systems: GPS, GLONASS, Galileo & more*. Wien: Springer.

Howind, J. (2005). Analyse des stochastischen Modells von GPS-Trägerphasenbeobachtungen. Deutsche Geodätische Kommission, No. C584, Verlag der Bayerischen Akademie der Wissenschaften, Munich.

IS-GPS-200E (2010). Navstar GPS space segment/navigation user interfaces. Interface Specification, IS-GPS-200, Revision E. Science Applications International Corporation GPSW SE&I, El Segundo, CA, 8 June.

Jordan, E. C., & Balmain, K. G. (1968). *Electromagnetic waves and radiating systems* (2nd ed.). Englewood Cliffs: Prentice Hall.

Landau, H. (2006). SNR data from the Trimble NetR5 and 4700 receivers. Personal communication on 19 Dec, Trimble Terrasat GmbH, Höhenkirchen-Siegertsbrunn, Germany.

Langley, R. B. (1997). *GPS receiver system noise. GPS World*, *8*(6), 40–45.

Lau, L., & Mok, E. (1999). Improvement of GPS relative positioning accuracy by using SNR. *Journal of Surveying Engineering*, *125*(4), 185–202. doi:10.1061/(ASCE)0733-9453(1999)125:4(185).

Luo, X., Mayer, M., & Heck, B. (2007). Bestimmung von hochauflösenden Wasserdampffeldern unter Berücksichtigung von GNSS-Doppeldifferenzresiduen. Schriftenreihe des Studiengangs Geodäsie und Geoinformatik, Band 2/2007, Karlsruher Institut für Technologie (KIT), KIT Scientific Publishing, Karlsruhe.

Luo, X., Mayer, M., & Heck, B. (2008a). Erweiterung des stochastischen Modells von GNSS-Beobachtungen unter Verwendung der Signalqualität. *Zeitschrift für Geodäsie, Geoinformation und Landmanagement (ZfV), 133*(2), 98–107.

Luo, X., Mayer, M., & Heck, B. (2008b). Improving the stochastic model of GNSS observations by means of SNR-based weighting. In: M. G. Sideris (Ed.), *Observing our changing Earth, Proceedings of the 2007 IAG General Assembly*, Perugia, Italy, 2–13 July, IAG Symposia, vol. 133, Berlin: Springer, pp. 725–734. doi:10.1007/978-3-540-85426-5_83.

Mader, G. L. (1992). Rapid static and kinematic Global Positioning System solutions using the ambiguity function technique. *Journal of Geophysical Research, 97*(B3),3271–3283. doi:10.1029/91JB02845.

Mayer, M. (2006). Modellbildung für die Auswertung von GPS-Messungen im Bereich der Antarktischen Halbinsel. Deutsche Geodätische Kommission, No. C597, Verlag der Bayerischen Akademie der Wissenschaften, Munich.

Mehaffey, J. (2011). Rain, snow, clouds and GPS reception. Available online at http://gpsinformation.net/gpsclouds.htm, accessed on 6 Feb, 2011.

Misra, P., & Enge, P. (2006). *Global Positioning System: Signals, measurements and performance* (2nd ed.). Lincoln: Ganga-Jamuna Press.

Rost, C., & Wanninger, L. (2009). Carrier phase multipath mitigation based on GNSS signal quality measurements. *Journal of Applied Geodesy*, *3*(2), 81–87. doi:10.1515/JAG.2009.009.

Rost, C., & Wanninger, L. (2010). Carrier phase multipath corrections based on GNSS signal quality measurements to improve CORS observations. In: *Proceedings of IEEE/ION PLANS 2010*, Indian Wells, CA, 4–6 May, pp. 1162–1167.

Satirapod, C., & Wang, J. (2000). Comparing the quality indicators of GPS carrier phase observations. *Geomatics Research Australasia*, *73*, 75–92.

Talbot, N. (1988). Optimal weighting of GPS carrier phase observations based on the signal-to-noise ratio. In: *Proceedings of the International Symposium on Global Positioning Systems*, Gold Coast, Australia, 17–19 Oct, 1988, pp. 4.1–4.17.

Trimble (1999). SNR conversions. Mail from Trimble support on 13 July, 1999, available online at http://gauss.gge.unb.ca/papers.pdf/SNR.memo.pdf, accessed on 8 June, 2012.

Ward, P. W., Betz, J. W., & Hegarty, C. J. (2006). Interference, multipath, and scintillation. In: E. D. Kaplan & C. J. Hegarty (Eds.), *Understanding GPS: Principle and applications* (2nd ed.), chapter 6, Norwood: Artech House.

Wieser, A., & Brunner, F. K. (2000). An extended weight model for GPS phase observations. *Earth, Planets and Space*, *52*(10), 777–782.